Investigations on the Redox Performance of Pure and Doped CeO_2 by Comparing Solid State Reaction and Pechini Synthesis

Alexander Bonk, Annika C. Maier, Dariusz Burnat, Ulrich F. Vogt and Andreas Züttel

Abstract Undoped and doped ceria were synthesized by a solid state reaction and a polymerized—complex method. Microstructural and phase development of $M_xCe_{1-x}O_{2-\delta}$ (M = Zr, Hf; $0 \leq x \leq 0.2$) were examined using X-ray diffraction and scanning electron microscopy. Redox properties were investigated by thermogravimetric analysis and a remarkable increase of the oxygen storage capacity of ceria with increasing dopant concentration was demonstrated. $Zr_xCe_{1-x}O_2$ and $Hf_xCe_{1-x}O_2$ solid solutions at x = 0.2 were shown to release double the amount of oxygen during reduction compared to undoped ceria. The solid state reaction synthesis produces materials with excellent redox performance up to 15 mol% dopant concentration and is otherwise equivalent with materials produced by Pechini synthesis.

1 Introduction

Solar thermochemical redox cycles based on metal oxides can be used to reduce H_2O or CO_2 to produce H_2 or CO, respectively [1, 2]. Due to its excellent thermodynamic and kinetic properties, CeO_2 is one of the most promising non-volatile metal oxides for this application [2–5].

A. Bonk (✉) · A.C. Maier · D. Burnat · U.F. Vogt · A. Züttel
Empa, Swiss Federal Laboratories for Materials Science and Technology,
Laboratory for Materials for Energy Conversion, 8600 Dübendorf, Switzerland
e-mail: Alexander.Bonk@empa.ch

A. Bonk · A.C. Maier · U.F. Vogt
Institute for Geo- and Environmental Science, Albert-Ludwigs-University Freiburg,
Crystallography, 79098 Freiburg i.Br., Germany

A. Züttel
École Polytechnique Fédérale de Lausanne (EPFL),
Institut des Sciences et Ingénierie Chimique, Lausanne, Switzerland

W. Udomkichdecha et al. (eds.), *Materials for Energy Infrastructure*,
DOI 10.1007/978-981-287-724-6_2

In a 2-step solar thermochemical cycle, CeO_2 releases oxygen from its lattice to form nonstoichiometric ceria when heated in a reducing atmosphere to above 1400 °C [3, 4] according to:

$$CeO_2 \rightarrow CeO_{2-\delta} + \frac{\delta}{2} O_2 \tag{1}$$

where δ is the extent of oxygen nonstoichiometry. The formed $CeO_{2-\delta}$ reacts with CO_2 and H_2O at ~1000 °C according to the following two steps:

$$CeO_{2-\delta} + \delta CO_2 \rightarrow CeO_2 + \delta CO \tag{2}$$

$$CeO_{2-\delta} + \delta H_2O \rightarrow CeO_2 + \delta H_2 \tag{3}$$

Stoichiometric CeO_2 is regained during oxidation thereby closing the redox cycle.

Controlling the thermodynamics, kinetics and the transport of concentrated solar energy to the reactant is essential in designing highly efficient ceria based redox systems [3]. It has been proposed that doping of CeO_2 with isovalent cations has a significant impact on its redox properties [6]. Extensive studies conducted on ceria-zirconia [7] and ceria-hafnia [8] solid solutions have shown a remarkable increase of oxygen storage capacity of ceria with increasing dopant concentrations. Materials used in these studies [7, 8] were produced by wet chemical methods. Doped ceria structures synthesized by solid state reaction (SSR) have not been investigated yet, to our best knowledge, despite the SSRs practical and economical relevance.

In this work, we compare $M_xCe_{1-x}O_{2-\delta}$ (M = Hf, Zr; $0 \leq x \leq 0.2$) produced by Pechini synthesis and by solid state reaction (SSR). Although the SSR is known to suffer from limited diffusion rates of dopants into the host lattice, it is practically relevant and allows economical up-scaling. The Pechini-derived materials, which provide high elemental homogeneity due to the mixing of precursors on an atomic scale, serve as reference materials. The phase purity, crystal structure, microstructure development and redox properties will be addressed.

2 Experimental

2.1 Solid State Reaction Synthesis (SSR)

Solid solutions of $M_xCe_{1-x}O_{2-\delta}$ (M = Hf, Zr; x = 0.05, 0.1, 0.15, 0.2) were synthesized using CeO_2 (Sigma Aldrich, 99.9 %, <5 μm) and stoichiometric amounts of HfO_2 (Alfa Aesar, 99.95 %) and ZrO_2 (TZ-0, 99.95 %, Tosoh, Japan). For thermal analysis porous samples were produced by mixing spherical carbon pore-forming (CPF) agent particles (0.4–12 μm particle size, HTW Hochtemperatur-Werkstoffe GmbH) with the metal oxide mixtures in a 1:5 mass-ratio prior to ball milling.

Deagglomeration and mixing of the metal oxides (+CPF) was carried out by conventional ball milling on a roller mill (ZOZ, RM1, Germany) for 24 h in polypropylene bottles using YSZ balls of 5 mm diameter (Tosoh, Japan) and distilled water. After 24 h the slurry was separated from the YSZ balls and dried at 85 °C for at least 12 h. Samples of 300 mg were pressed uniaxially at 5 MPa in a Ø10 mm pressing die and sintered in a furnace (Carbolite HTF 17/10) at 1600 °C for 5 h prior to any measurement leading to removal of all carbon species. During sintering samples were placed on an alumina plate and a ceria powder bed to avoid reaction between samples and the alumina plate.

2.2 Pechini Synthesis

$Zr_xCe_{1-x}O_2$ and $Hf_xCe_{1-x}O_2$ solid solutions were synthesized from a polymerized complex method. Cerium (IV) ammonium nitrate (Alfa Aesar, 99.9 %) and $ZrO(NO_3)_2$ (Alfa Aesar, 99.9 %) or $HfCl_4$ (Alfa Aesar, 99.9 %) respectively were dissolved in deionized water (75 ml). Anhydrous citric acid (CA) (Sigma-Aldrich, 99.5 %) was added to 1,4-butanediole (BD) (Sigma-Aldrich, 99 %) and stirred at 100 °C until all citric acid was dissolved. The aqueous solution containing the dissolved metal salts was added to the CA-BD mixture and heated to 150 °C to promote the esterification reaction. The gained honey-like polymer was dried at 80 °C for 24 h, transferred to an alumina crucible and fired for 10 h at 700 °C in a constant air flow to remove all organic compounds. For thermal analysis the pre-calcined powders were ground with CPF in a agate mortar. Pressing and sintering for 5 h at 1600 °C were carried out applying the same conditions used for the SSR samples.

2.3 Characterization Methods

X-ray diffraction (XRD) patterns were recorded on a Bruker D8 (Parallel Beam) using Cu-Kα radiation in a 2θ range of 10–110° (step size 0.014°, scan speed 1°/min). XRD pattern of Pechini samples were recorded after precalcination (700 °C, 10 h) as well as after sintering (1600 °C, 5 h). XRD analysis was performed only on sintered (1600 °C, 5 h) samples. Rietveld refinement was conducted using the Bruker Topas 4.2 software. The average crystallite size was calculated from the reflex broadening for all reflexes of the fcc structure using Scherrer's equation.

SEM was carried out on a FEI ESEM CL30 using high vacuum secondary electron and back scattered (BSE) electron-detectors. Samples were polished, thermally etched (1500 °C, 30 min) and sputtered with Pd/Au prior to the measurements.

A Netzsch 409 CD was used for thermal cycling experiments. Cylindrical pellets of 290 ± 10 mg were reduced under Ar 5.0 atmosphere for 2 h at 1500 °C to reach thermodynamic equilibrium during reduction. The oxygen partial pressure was

measured at the outlet using a gas chromatograph (Varian 490) and was in the range of $P_{O_2} \sim 2 \times 10^{-4}$ atm. Oxidation was carried out at 1000 °C under 0.5 atm CO_2 (4.8) in Ar (5.0) atmosphere. Two successive redox cycles were performed for each sample.

3 Results and Discussion

3.1 Phase Development

For all Pechini samples pre-calcination leads to the formation of fcc structures that belong to the Fm-3m space group (Fig. 1a, b). A detailed analysis of FWHM shows that increasing Hf and Zr concentrations result in broader peaks mainly caused by smaller crystallite sizes (Fig. 1c). This trend is attributed to the presence of Zr^{4+} (0.84 Å [9]) and Hf^{4+} (0.83 Å [9]) cations with a smaller ionic radius than Ce^{4+} (0.97 Å [9]). A substitution of Ce^{4+} with Zr^{4+}/Hf^{4+} distorts the ceria lattice, reduces the relative degree of crystallinity and is responsible for the present peak asymmetry.

After sintering for 5 h at 1600 °C, a peak shift to higher 2Θ angles with increasing dopant concentrations is observed (Fig. 2a, b). We attribute this to the substitution of Ce^{4+} by smaller Zr^{4+} or Hf^{4+} cations. The same conclusion is drawn with respect to SSR synthesized samples, for which a peak shift with increasing dopant concentrations was observed after the same heat treatment (data not shown). Both synthesis routes finally lead to symmetrical and narrow reflections indicating a high relative degree of crystallinity [10].

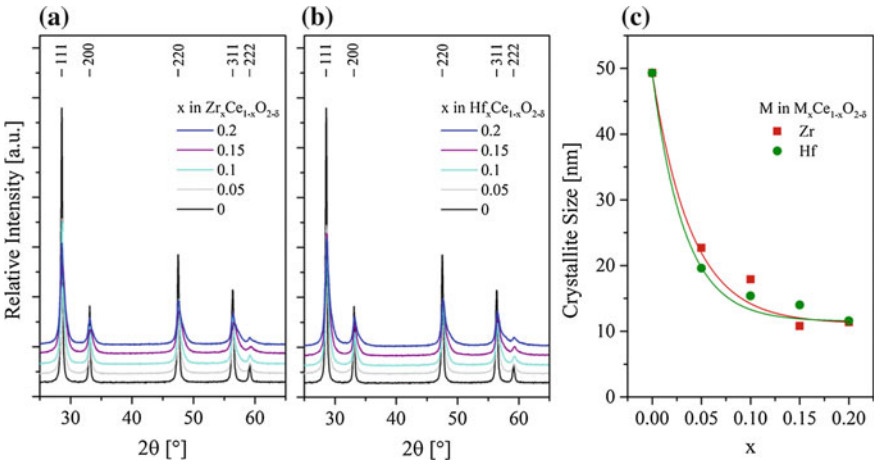

Fig. 1 XRD pattern and crystallite sizes of Pechini synthesized $M_xCe_{1-x}O_{2-\delta}$ (M = Hf, Zr; $0 \leq x \leq 0.5$) after calcination for 10 h at 700 °C. Y—axis offset is added for clarity

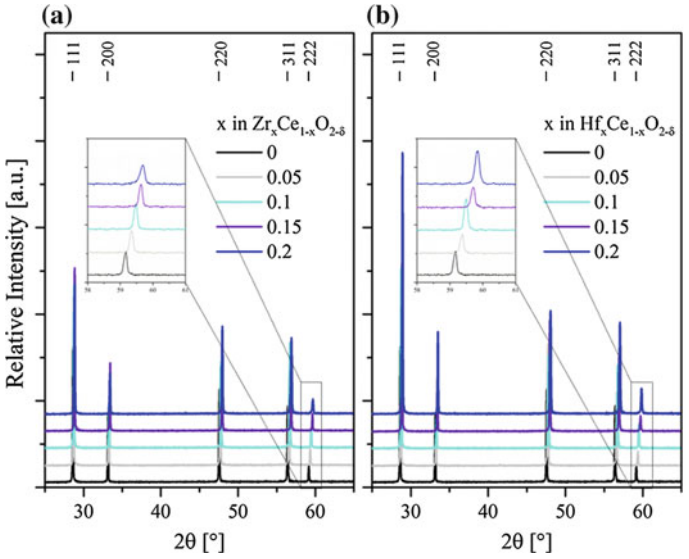

Fig. 2 Diffractograms of the $M_xCe_{1-x}O_{2-\delta}$ samples produced by Pechini synthesis after 5 h sintering at 1600 °C. Y—axis offset is added for clarity

Since both synthesis routes lead to the formation of solid solutions of $M_xCe_{1-x}O_{2-\delta}$ (M = Zr, Hf; $0 \leq x \leq 0.2$) a correlation of specific redox properties to the cubic lattice parameter (depending on Zr^{4+}/Hf^{4+} concentrations) and the synthesis route can be established as discussed later [7].

3.2 *Microstructural Development*

The influence of the dopants on the microstructural development during sintering was investigated using undoped and 10 mol% doped solid solutions. SEM images of the sintered (1600 °C, 5 h) samples show a monomodal grain size distribution as presented in Fig. 3. In undoped ceria produced by SSR and Pechini synthesis inter- and intragranular pores are present owing to rapid grain boundary diffusion causing pore-boundary separation as described by Brook [11].

For SSR samples the amount of intragranular pores is similar in undoped and doped ceria. Accordingly, the boundary velocity in all samples must be larger than the pore velocity during sintering of all $M_xCe_{1-x}O_{2-\delta}$ solid solutions [12]. Obviously, the sintering of CeO_2 is not inhibited by the addition of ZrO_2 or HfO_2 using the SSR synthesis.

For both synthesis methods Hf and Zr doping decreases the average grain size as compared to undoped CeO_2. This is especially desirable for materials used in solar reactors, where sintering effects induced by grain growth suppress the kinetics of the CO/H_2 production reaction (Eqs. (2) and (3)) [4].

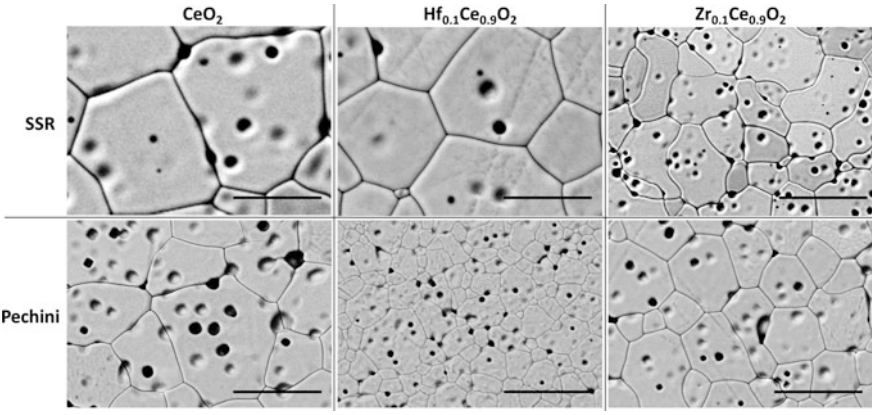

Fig. 3 Micrographs of undoped and doped ceria after sintering (5 h at 1600 °C), polishing and thermal etching (1500 °C for 30 min). Scale bars equal 40 μm

The reference Pechini samples exhibit microstructures with inter—and intragranular porosity. They have smaller grain sizes compared to SSR samples owing to their initially small particle size. However, the grain sizes are above 10 μm for all Pechini samples.

The long term treatment (cycling) at high temperatures is expected to result in microstructures that are similar in Zr-, Hf- and undoped Ceria owing to their similar sintering properties and microstructure development presented here. However, a more detailed insight into crystallization as a function of dopant concentration, temperature and synthesis route is required which is beyond the scope of this study.

3.3 RedOx Property Investigations

Thermal cycling experiments are carried out simulating the solar reactor conditions. As demonstrated in Fig. 3, the SSR and Pechini samples exhibit similar morphologies after sintering.

Mass changes during reduction and oxidation of ceria are correlated solely with oxygen release/uptake, respectively. The oxygen release is proportional to the nonstoichiometry δ in $CeO_{2-\delta}$ during reduction. The mass gain is directly proportional to the amount of fuel (CO) produced (Eq. (2)).

3.3.1 Zirconia Doped Ceria

The O_2 release during reduction and CO generation during oxidation of $Zr_xCe_{1-x}O_{2-\delta}$ produced by SSR is shown in orange in Fig. 4. With increasing Zr concentration an almost linear increase of O_2 release and CO generation is observed. For 20 mol%

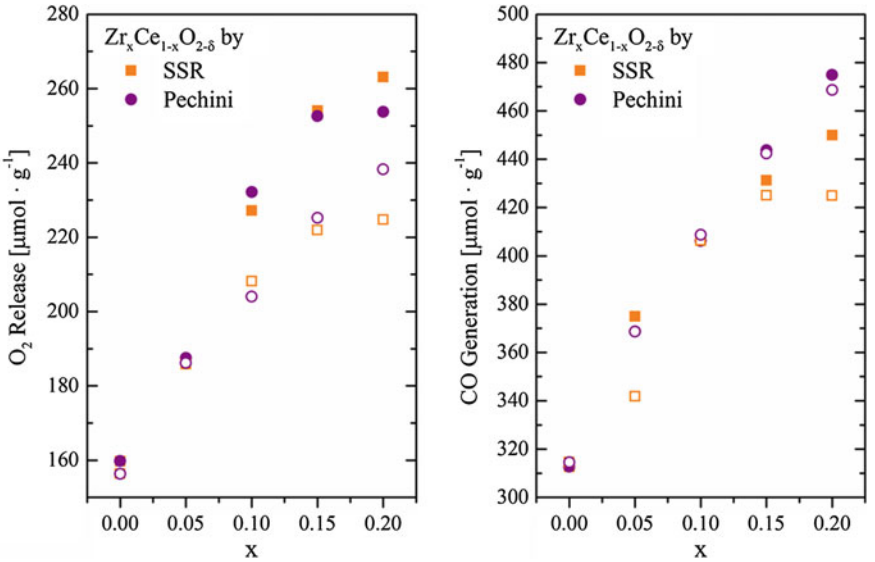

Fig. 4 The O_2 and CO release rates of $Zr_xCe_{1-x}O_2$ ($0 \leq x \leq 0.2$) from two successive reduction and oxidation cycles at 1500 and 1000 °C respectively. *Closed symbols* represent the first, *open symbols* the second cycle. Values are taken from points of thermodynamic equilibrium (mass at steady state)

Zr doped ceria the O_2 release is increased by 60 % as compared to undoped CeO_2. The successive CO release is ~55 % higher than in undoped ceria. During the second cycle a slight decrease of both O_2 release and CO generation rate is observed. The overall trend however remains linear with increasing dopant concentrations up to x = 0.15. Pechini synthesized samples (purple) show a similar redox behavior. The O_2 release and CO generation rates increase linearly with increasing Zr concentration. In the second cycle these trends remain linear up to 20 mol% Zr concentration.

Constant CO generation rates during two successive redox cycles arise from structural as well as phase stability of the samples. This differs from other reports on the same material types [13, 14] in which a strongly decreasing reduction and oxidation extent during successive cycles was reported. Excellent stability of presented materials (SSA and Pechini) at higher temperatures is attributed to hindered sintering effects, which originate from initially coarser-grained structures [13]. It could be demonstrated that SSR and Pechini samples are equivalent up to Zr concentrations of 15 mol%.

The scattering of data during the first and the second redox cycle (Fig. 4) has been described in other studies. Namely, differences in the heating time are shorter during the second cycle [15] and sintering effects can lead to coarsening of the microstructure [3, 8] however, stabilization of the redox performance is typically observed after a few cycles [3, 8].

3.3.2 Hafnia Doped Ceria

The $Hf_xCe_{1-x}O_{2-\delta}$ solid solutions show similar trends as compared to $Zr_xCe_{1-x}O_{2-\delta}$. For SSR samples the O_2 release rates increase linearly with increasing dopant concentration during the first cycle (Fig. 5). The O_2 release is 85 % higher at x = 0.2 while for the same Pechini sample the extent of reduction is doubled in comparison to undoped ceria. During the second cycle the O_2 release of both SSR and Pechini (x = 0.2) decreases by ~40 % in relation to the first cycle.

At 20 mol% Hf doping the CO release is in the same range as for 10 mol% Hf doping for both SSR and Pechini samples. Stoichiometrically the CO generation rates should double the precedent O_2 release rates (Eqs. (1) and (2)). However, only ~60 % of the initial oxidation state is gained during oxidation of $Hf_{0.2}Ce_{0.8}O_{2-\delta}$ regardless of the synthesis route.

We rule out that sintering effects cause the decreasing reduction and oxidation extents. Typically, losses due to sintering effects are reported to be below 10 % [3, 4]. We infer that the significant thermodynamic change is due to a phase transition in $Hf_{0.2}Ce_{0.8}O_{2-\delta}$. For chemically similar $Zr_xCe_{1-x}O_{2-\delta}$ a phase transition from cubic to tetragonal (c-t″) at x = 0.2 results in decreasing reduction enthalpies and thus decreasing redox performance [7]. The phase transition is induced by small Zr^{4+} cations that prefer 7-fold coordination, leading to oxygen displacement along the c-axis [7]. For Hf doped ceria the thermodynamic behavior of tetragonal phases has

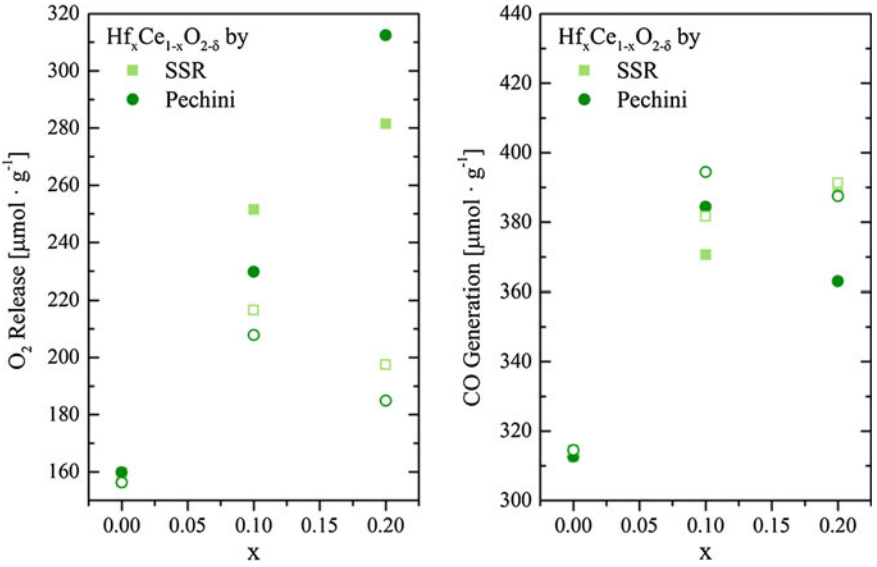

Fig. 5 O_2 and CO release rates of $Hf_xCe_{1-x}O_2$ ($0 \leq x \leq 0.2$) from two successive reduction and oxidation cycles at 1500 and 1000 °C respectively. *Closed symbols* represent the first, *open symbols* the second cycle. Values are taken from points of thermodynamic equilibrium (mass at steady state)

not been described yet. Due to the chemical similarity and similar ionic radius of Hf^{4+} and Zr^{4+} we expect similar phase transitions and thus thermodynamic trends.

The redox cycles presented demonstrate that SSR sample are equivalent with reference materials up to 15 mol% Zr concentration. For Hf doped ceria, equivalency during the second redox cycle for both, 10 and 20 mol% dopant concentration is obvious. However, detailed investigations are required to elucidate the connection between phase transitions in Hf doped ceria and thermodynamic performance which differs from Zr doped ceria. For the evaluation of possible redox materials other factors have to be further understood. For example, more accurate equilibrium measurements that relate P_{O_2} and nonstoichiometry and more fundamental kinetic studies are required to make a fair comparison between all samples considered. Specific microstructures and morphologies have to be investigated with regard to reactor conditions since they have a significant impact on both kinetics and thermodynamics. A more specific analysis is required to understand the final performance of redox materials in the overall process.

4 Conclusion

Doping of ceria with tetravalent dopants was investigated and two synthesis methods were compared. The SSR and Pechini synthesis demonstrated effective incorporation of dopants into the ceria lattice and only minor influence of dopants on the microstructure and grain size evolution of the ceramic.

Single phase fcc structures were formed up to x = 0.2 in $M_xCe_{1-x}O_{2-\delta}$ (M = Zr, Hf) using both synthesis routes as proven by XRD and SEM. Incorporation of dopants was reflected by a decreasing lattice constant with increasing dopant concentrations.

The oxygen storage capacity of doped and undoped ceria was tested using thermogravimetric analysis. The O_2 evolution and successive CO generation rates linearly increase with increasing x in $Zr_xCe_{1-x}O_{2-\delta}$ solid solutions. Constant oxidation rates over two successive cycles reflected the minor influence of sintering effects on the overall performance of Zr doped ceria.

Pechini synthesized $Hf_xCe_{1-x}O_{2-\delta}$ show the same trend during the first reduction step as compared to $Zr_xCe_{1-x}O_{2-\delta}$. During the second cycle a significant decrease of both O_2 release and CO generation rate was observed. The phase segregation of Hf enriched phases in $Hf_{0.2}Ce_{0.8}O_{2-\delta}$ is likely but has to be approved in further studies.

Overall, the SSR samples show similar OSCs in both Zr and Hf doped ceria systems compared to reference Pechini samples.

Using both synthesis methods chemically identical materials can be synthesized yielding similar OSCs and kinetics during reduction and oxidation. The SSR synthesis shows no drawbacks in terms of sintering or oxygen storage capacity making it attractive for the synthesis of ceria for larger scale redox applications.

Acknowledgments We gratefully acknowledge the financial support by the Swiss Competence Center Energy & Mobility (Proposal # 701) and the fruitful discussion with members of the COST Action CM1104 during the 3rd General Meeting in Barcelona, November 2014.

References

1. Steinfeld A (2005) Solar thermochemical production of hydrogen—a review. Sol Energy 78(5):603–605
2. Meier A, Steinfeld A (2010) Solar thermochemical production of fuels. Adv Sci Tech 74:303–312
3. Furler P, Scheffe JR, Marxer D, Gorbar M, Bonk A, Vogt UF, Steinfeld A (2014) Thermochemical CO_2 splitting via redox cycling of ceria reticulated foam structures with dual-scale porosity. Phys Chem Chem Phys 16:10503–10511
4. Furler P, Scheffe JR, Steinfeld A (2012) Syngas production by simultaneous splitting of H_2O and CO_2 via redox reactions in a high-temperature solar reactor. Energy Environ Sci 5 (3):6098–6103
5. Chueh WC, Falter C, Abbott M et al (2010) High-flux solar-driven thermochemical dissociation of CO_2 and H_2O using nonstoichiometric ceria. Science 330:1797–1802
6. Scheffe JR, Steinfeld A (2012) Thermodynamic analysis of cerium-based oxides for solar thermochemical fuel production. Energy Fuels 26(3):1928–1936
7. Kuhn M, Bishop SR, Rupp JLM, Tuller HL (2013) Structural characterization and oxygen nonstoichiometry of ceria-zirconia ($Ce_{1-x}Zr_xO_{2-\delta}$) solid solutions. Acta Mater 61(11):4277–4288
8. Scheffe JR, Jacot R, Patzke GR, Steinfeld A (2013) Synthesis, characterization, and thermochemical redox performance of Hf^{4+}, Zr^{4+}, and Sc^{3+}Doped ceria for splitting CO_2. J Phys Chem C 117(46):24104–24114
9. Shannon R (1976) Revised effective ionic radii and systematic studies of interatomic distances in halides and chalcogenides. Acta Crystallographica Section A 32(5):751–767
10. Akurati KK, Vital A, Fortunato G, Hany R, Nueesch F, Graule T (2007) Flame synthesis of TiO_2 nanoparticles with high photocatalytic activity. Solid State Sci 9(3–4):247–257
11. Brook RJ (1969) Pore-grain boundary interactions and grain growth. J Am Ceram Soc 52(1):56–57
12. Jud E, Huwiler CB, Gauckler LJ (2006) Grain growth of micron-sized grains in undoped and Cobald Oxide Doped ceria solid solutions. J Ceram Soc Jpn 114(11):963–969
13. Abanades S, Le Gal A (2012) CO_2 Splitting by thermo-chemical looping based on $Zr_xCe_{1-x}O_2$ oxygen carriers for synthetic fuel generation. Fuel 102:180–186
14. Le Gal A, Abanades S, Flamant G (2011) CO_2 and H_2O splitting for thermochemical production of solar fuels using nonstoichiometric Ceria and Ceria/Zirconia solid solutions. Energy Fuels 25(10):4836–4845
15. Le Gal A, Abanades S, Bion N, Le Mercier T, Harlé V (2013) Reactivity of doped ceria-based mixed oxides for solar thermochemical hydrogen generation via two-step water-splitting cycles. Energy Fuels 27(10):6068–6078

http://www.springer.com/978-981-287-723-9

Materials for Energy Infrastructure

Udomkichdecha, W.; Mononukul, A.; Böllinghaus, Th.; Lexow, J. (Eds.)

2016, VIII, 124 p. 52 illus., 35 illus. in color., Hardcover
ISBN: 978-981-287-723-9